

Optimization of Centrifugal Pump Based on Impeller-Volute Interactions

Maitrik Shah*, Beena Baloni, Salim Channiwala

Department of Mechanical Engineering, Sardar Vallabhbhai National Institute of Technology, Gujarat, India

Received 19 September 2021; received in revised form 06 December 2021; accepted 07 December 2021

DOI: <https://doi.org/10.46604/aiti.2022.8509>

Abstract

The design and off-design performance of a centrifugal pump largely depends on geomechanical parameters. This study aims at enhancing the performance by optimizing three geomechanical parameters of impeller-volute interactions. The present optimization is carried out using the Taguchi method combined with a numerical approach. A comparison between the base and optimized pumps is presented under the design and off-design conditions based on numerical and experimental analyses. The numerical results reveal that, compared to the base pump, the optimized pump shows the improved performance through uniform pressure distribution in the impeller, the reduced low-pressure region towards a blade's leading edge, and the stable total pressure at the impeller-volute interaction zone. The experimental results suggest that the optimized pump covers a wider range of operation, and its best efficiency point (BEP) is 10%, 5%, and 12% higher in flow rate, head, and efficiency, as compared to the base one.

Keywords: centrifugal pump, optimization, design of experiment, experimental analysis, numerical analysis

1. Introduction

A centrifugal pump, which is the highly recommended and utilized pump to date, is a principal member of the power-consuming turbomachine family. It is widely used in industrial areas such as water, processing, and chemical industries to increase fluid pressure. It occupies a large share of electricity consumption of the world's total generated electricity. Therefore, high pump efficiency is essential in reducing power requirements and reaping economic benefits. The constructive geometry of the centrifugal pump is developed with its rotor (impeller) and stator (volute). The fluid energy is enhanced by the conversion of mechanical work in the impeller, whereas the volute does energy transformation to further enhance the pressure energy of the fluid. There are two methods for improving the centrifugal pump performance in general. The first is to investigate the impact of a single parameter or structure. The second is to examine the combined effects of various parameters on the pump performance using computational equations or algorithms.

Many studies have concentrated on enhancing the pump efficiency by optimizing the construction of centrifugal pumps, which allows for the hydraulically smooth fluid flow and mechanically stiff operating behavior. The impeller and volute in a centrifugal pump assembly can significantly influence the pump performance. Researchers have conducted the impeller optimization followed by the volute or diffuser optimization, but the impeller and volute optimization have never been conducted together. Also, in the studies of impeller optimization, the researchers concentrated on the main parameters of blades, i.e., the meridional shape, wrap angle, thickness, total number, inlet-outlet angle, width at inlet-outlet, profile curvature, shape of leading edge (LE), and trailing edge (TE). For the volute optimization, the researchers focused on the volute inlet width, cross-section shape, tongue angle, outlet position, and diffuser cone angle.

* Corresponding author. E-mail address: maitrikshah2006@gmail.com

Tel: +91-972-5852858

In the impeller optimization design, the pump hydraulic performance is more influenced by the number of blades and the exit blade angles. Literature suggests that the generated head is linearly proportional to the number of blades and not apparent with the impeller outlet width [1]. The pump's flow rate decreased due to the increased blockage areas by increasing the blade numbers of the impeller [2]. Also, the friction and mixing losses are increased with more blades. Elyamin et al. [3] found that the pump performance was improved with seven blades than nine blades in the impeller. The blades with small exit angles outperform the blades with large exit angles. The wear on the blade outlet can be diminished with the reduced blade exit angles [4]. The increment in TE blade angle resulted in 2.32% higher hydraulic efficiency [5]. The rounding with a fillet radius of 3.5 mm at TE improved the pump efficiency by more than 10% for a high-flow centrifugal mixed flow pump [6]. The bezier curve optimization in impeller design enhanced the efficiency of a double suction centrifugal pump [7].

Subsequently, bee colony algorithms improve the impeller design by optimizing the structural characteristics of the impeller's inlet-outlet, such as diameter, width, and blade angle. Derakhshan et al. [8] found that the pump efficiency was enhanced by 3.59% for the optimized centrifugal pump. In the work of Xu et al. [9] and Liet al [10], the orthogonal table method was used to optimize the centrifugal pump performance, which improved efficiency and reduced critical net positive suction head (NPSH_c) by 3.09% and 1.45 meters, respectively. Sekino et al. [11] performed the optimization design for the double suction centrifugal pump with the help of design of experiments (DoE) and computational fluid dynamics (CFD). The results showed a 4% rise in efficiency.

In addition, the optimization of volute reduced the internal cross-sectional area to 90% of the primary volute, resulting in an increment in head and efficiency for the optimized impeller model [12]. A low specific speed centrifugal pump with several volute configurations (spiral, concentric, and double) and two distinct impeller designs (four and five blades) was evaluated to optimize the impeller and volute together. Baun et al. [13] found a 5% head gain and a corresponding efficiency gain for a five-blade impeller with spiral volute. In the radial flow low specific speed (N_s) centrifugal pump, the generated radial force was high at a high flow rate. Therefore, Stepanoff [14] suggested a volute design with a circular cross-section that provided better hydraulic performance and lower radial force, especially at a high flow rate [15]. The mixing losses at the impeller-volute interaction zone were measured by the entropy generation and minimized by the optimum selection of the design variables established with the help of an orthogonal matrix [16].

The literature shows that understanding and handling the design parameters can give a better and more optimized design. However, there is a need to focus on the combined effect of the impeller and volute design parameters for optimizing the centrifugal pump. Therefore, the present study incorporates numerical and experimental analyses to optimize the pump performance using Taguchi's orthogonal techniques, based on the parameters such as the volute inlet width to impeller outlet width ratio b_3/b_2 , number of blades Z , and blade outlet angle β_2 .

2. Numerical Simulation

The numerical analysis approach with the help of the Reynolds averaged Navier-Stokes (RANS) equation is a widely used tool for visualizing the flow inside the 3D flow domain. The present numerical analysis is carried out for a single-stage centrifugal pump having a specific speed of 22.5 (metric unit). Its impeller and volute are designed based on meridional plane velocity and constant velocity methods, respectively. The geometrical model of the single-stage radial flow centrifugal pump follows ISO 2858 [17]. The main geometric parameters of the impeller and volute are obtained using the Creo Parametric tool and are shown in Table 1. The computational model consists of an impeller, volute, suction pipe, and discharge pipe, as shown in Fig. 1.

The numerical analysis is performed with the help of Ansys commercial software packages for grid generation and CFD setup. The unstructured computational grid is selected due to less computational time and is developed separately by the Ansys meshing tool for suction pipe, impeller, volute, and discharge pipe. Special attention is given to mesh quality for impeller and

volute grid generation. The inflation method is used for mesh generation at the fluid-structure interaction areas for calculating the structure’s effect on the fluid flow region. The accuracy of the numerically obtained results depends on the quality of the computing grid, especially in the situation of dominating the decelerating flow in the pump. The grid refining increases the computational time and is critical near the impeller wall region due to mesh freezing. In the present work, the fluid domain has y^+ values of 20 to 50 in critical areas for better accuracy of findings [18]. The expansion ratio is 1.5 near the impeller and volute wall, and the maximum aspect ratio is 150. The first layer height is $10e-4$ m close to the wall, and the number of inflation layers is 10.

The grid convergence study is carried out with eight different grids (0.5, 0.75, 1.5, 2.15, 1.5, 3.01, 3.5, and 4 million), as shown in Fig. 2. The grid convergence test is performed between the pump efficiency and the grid elements [18]. Fig. 2 reveals that the efficiency variation is within 0.9% for a 3.5 million grid. The larger mesh sizes increase the computational time with no significant change in pump efficiency. Therefore, 3.5 million grid elements are selected for simulation.

Multiple frames of reference are applied to stationary and rotating fluid domains. The suction pipe, volute, and discharge pipe are set as stationary frames, and the impeller is designated as a rotating frame at 2930 rpm. The interface between two stationary components is set to the general grid connection, and the stationary-rotary domain is set to the rotor-stator “frozen rotor” interface [18]. A fluid is defined as water at 25 °C. The boundary conditions are applied as total pressure (1.01325 bar) at the inlet and mass flow rate (13.8611 kg/sec) at the outlet [19]. A frozen rotor is used to define the sliding interface. The control volume’s surface roughness is set at 50 μ m. The pump’s physical surfaces are configured as no-slip walls [20], and the conventional wall function is applied to the turbulent flow near-wall. The RNG k- ϵ model is used for the present analysis [19]. For the convergence criterion, the equation of residual’s root-mean-square (RMS) value for all sets of the RANS equation must be at least $1.0E-6$. The hydraulic design is created to provide a broader operational range without recirculation and to achieve the operating range of best efficiency point (BEP). When $Q \ll Q_{opt}$, CFD studies are required for higher partial flow rates. The variable mass flow is applied to an outlet boundary condition for a full outlet diameter (OD) of impeller. The numerical results are discussed and compared with experimental results in section 5.

Table 1 Centrifugal pump parameters

Parameters	Value	Parameters	Value
Impeller suction eye diameter, D_1 (mm)	80	Impeller blade number, Z (nos.)	7
Impeller outlet diameter, D_2 (mm)	172	Impeller blade thickness, δ (mm)	4
Impeller outlet width, b_2 (mm)	14	Volute base diameter, D_3 (mm)	189
Impeller blade inlet angle, β_1 (°)	24	Volute inlet width, b_3 (mm)	23
Impeller blade outlet angle, β_2 (°)	36	Volute tongue angle, ϕ_o (°)	24
Impeller blade wrap angle, ϕ (°)	127	Volute outlet diameter, D_d (mm)	65

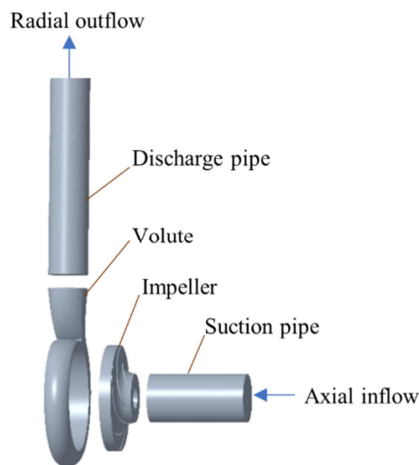


Fig. 1 The fluid domain of centrifugal pump

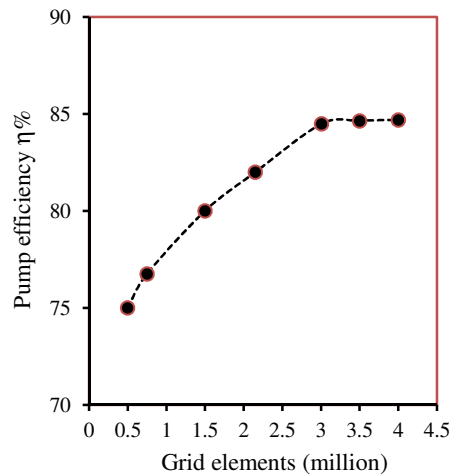


Fig. 2 Grid convergence test

3. Orthogonal Optimization

Taguchi's orthogonal array-based DoE technique is used to optimize the centrifugal pump model. The orthogonal table approach helps analyze the impact of specified parameters on the model. The principle of this approach is to determine a few parameters from experimental factors through an orthogonal array and simulate the results. These results are based on the effect of each parameter on the aggregate findings and the selection of the optimal parameter combination. In the current study, the performance of the base pump can be improved by a steeper performance curve. It can be achieved by modifying the blade number, impeller blade outlet width, and blade outlet angle [21].

The radial and semi-axial impellers (with a specific speed, $10 < n_q < 120$) are designed with 5 to 7 blades [21]. The small blade number means minor blockage due to blade thickness. The small values of blade number reduce the power overload and increase the pump efficiency. The small blade number also decreases the pump shut-off head. Therefore, the blade numbers Z selected for the current study are 5, 6, and 7.

The outlet angles β_2 of radial impellers with 5 to 7 blades are commonly in the range of 12° to 45° , including the deviation angle (predominantly 19° to 36°) [21]. Matching outlet blade angle and outlet width is an optimization task for increasing the efficiency and stability of the Q-H curve. The lower the impeller blade outlet angle, the steeper the performance characteristics and the lower the impeller flow coefficient. The selected blade angles β_2 in the current optimization study are 12° , 19° , and 36° .

The optimized opening width of the volute inlet and impeller outlet will reduce shock losses. Gülich [21] has suggested that the volute inlet width to impeller outlet width ratio b_3/b_2 should be in the range of 1.25 to 2.5. Thus, in the present optimization study, the proportion of b_3/b_2 is selected in the range of 1.64, 2, and 2.33.

The DoE techniques are used to create the orthogonal tables of the three chosen parameters. Table 2 shows the selected three distinct levels for each element. Nine groups of orthogonal test methods are built up according to the L_9 orthogonal table and are represented in Table 3. A numerical analysis is performed in Ansys CFX for nine orthogonal design scheme parameters. The numerical results are utilized to determine the best parameter combinations. Table 4 shows the head, efficiency, and percentage of total pressure loss in the volute for nine orthogonal design methods. The numerical findings are used to determine the optimal combination of the lowest and highest best parameters, known as the S/N ratio, which is expressed by Eqs. (1) and (2), respectively. The response table for each quality characteristic is prepared to find the best combination of parameters depending on each quality characteristic's S/N ratio and contribution, as shown in Table 5.

$$S/N = -10 \log \frac{1}{n} (\sum y^2) \quad (1)$$

$$S/N = -10 \log \frac{1}{n} \left(\sum \frac{1}{y^2} \right) \quad (2)$$

The response table for each quality characteristic is prepared to find the best combination of parameters depending on each quality characteristic's S/N ratio and contribution, as shown in Table 5. The sequence in which parameters have an impact on head, efficiency, and volute loss follows A3-B3-C1, A3-B1-C2, and A1-B1-C1, respectively. The results of all three configurations are compared with numerical simulation. The maximum centrifugal pump efficiency with minimum total pressure loss in volute is the selection criteria for the optimal sets. Therefore, the minimum losses are obtained with the combination of A1-B1-C1. The change in head, efficiency, and total pressure drop occurs in volute for A3-B3-C1 (+2.9%, -1.06%, and +17.63%) and A3-B1-C2 (+3.8%, -1.29%, and +12.12%), as compared to the optimum combination parameters A1-B1-C1. The uniform flow results in an efficient flow. The optimized models propose the ratio of volute inlet width to impeller outlet width $b_3/b_2 = 2$, blade outlet angle $\beta_2 = 19^\circ$, and blade number $Z = 6$.

Table 2 Factor levels in orthogonal experiments

Level	Factor		
	A	B	C
	Z (nos.)	b_3/b_2	β_2°
1	6	2	19
2	5	1.64	12
3	7	2.33	36

Table 3 Design of an orthogonal table

Scheme	Serial number			Design parameters		
	A	B	C	Z (nos.)	b_3/b_2	β_2°
1	A1	B1	C1	6	200	19
2	A1	B2	C2	6	167	12
3	A1	B3	C3	6	233	36
4	A2	B1	C2	5	200	12
5	A2	B2	C3	5	167	36
6	A2	B3	C1	5	233	19
7	A3	B1	C3	7	200	36
8	A3	B2	C1	7	167	19
9	A3	B3	C2	7	233	12

Table 4 Numerical results of orthogonal designs

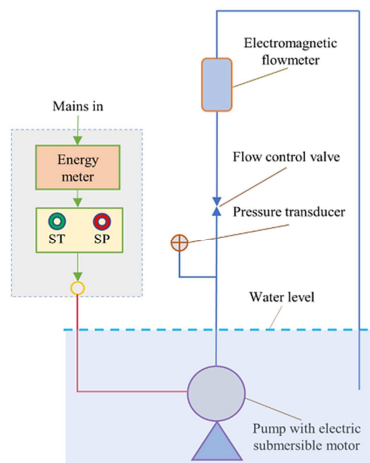
Scheme	Head (m)	Efficiency η (%)	Total pressure drops in volute (%)
1	41.97	85.16	6.35
2	40.34	83.76	6.83
3	42.63	81.32	8.55
4	40.68	85.88	6.97
5	40.54	82.31	8.23
6	40.11	85.09	6.80
7	39.98	85.09	7.34
8	45.21	83.55	7.15
9	44.35	84.95	7.71

Table 5 Response table for different quality characteristics

Levels	Maximum variation in the head (H) at the pump outlet			Maximum variation in the pump efficiency η (%)			Minimum variation in the total pressure P_o (%) loss inside the volute		
	A	B	C	A	B	C	A	B	C
1	32.39	32.23	32.54	38.42	38.63	38.55	-17.13	-16.74	-16.60
2	32.14	32.46	32.41	38.53	38.40	38.57	-17.27	-17.36	-17.10
3	32.69	32.53	32.26	38.54	38.46	38.37	-17.38	-17.68	-18.09
Delta	0.56	0.30	0.28	0.12	0.22	0.20	0.25	0.93	1.49
Rank	1	3	2	3	1	2	3	2	1
% Contribution	1	0.55	0.50	0.52	1	0.91	0.17	0.63	1

4. Experimental Test Setup

Experimental analysis of the centrifugal pump is carried out in submerged conditions as per ISO 9906 [22]. Fig. 3 represents a line diagram for the experimental setup and the tested centrifugal pump. The total head is measured by a pressure transducer installed before the valve. An electromagnetic flowmeter is used to measure the flow and is installed after the valve in the discharge line. The centrifugal pump is driven by an electric motor having a rated capacity of 415 voltage, 15 hp power output, and 2930 rpm. Table 6 shows the specifications of the instruments used for the experimental test setup.



(a) Line diagram of the experimental setup

(b) Tested centrifugal pump

Fig. 3 Experimental setup

Table 6 Specification of instruments

Measured parameter	Equipment name	Range	Least count	Accuracy
Pressure	Pressure transducer	0 to 5 bar	0.001	$\pm 0.2\%$
Flow rate	Electromagnetic flowmeter	0 to 217 m ³ /hr	0.06	$\pm 0.2\%$
Voltage	Voltmeter	50 to 450 V	0.01 V	$\pm 0.2\%$
Power factor, Cos ϕ	Cos phi meter	0.1 to 0.99	0.001	$\pm 0.1\%$
Current	Ammeter	0.250 A to 80 A	0.001 A	$\pm 0.2\%$
Watt	Energy meter	24 W to 24 kW	1 W	$\pm 0.2\%$
Shaft speed	Slip speed meter	1800 to 3000 rpm	1 rpm	$\pm 0.2\%$

The uncertainty in the overall measured efficiency is calculated by the Kline and McClintock uncertainty method [23]. The uncertainty in the overall efficiency is $\pm 2.24\%$ and within the permissible limit, i.e., $\pm 4.0\%$, as per ISO 9906 Grade 2 [22]. The repeatability of the experimental setup is checked and found in an acceptable range of 95% confidence limits.

5. Results and Discussion

Taguchi's orthogonal array-based design of experiment technique and Ansys CFX simulation are performed to optimize the selected base centrifugal pump. Based on the optimization results, a further comparison is made between the base and optimized case under the design and off-design conditions. The characteristics of pump performance are measured and plotted for both the pumps based on the results of numerical simulation and experimental analysis. At first, the numerical simulation for the base and optimized pump are carried out at $0.6 Q_d$, $0.8 Q_d$, $1.0 Q_d$, and $1.2 Q_d$. The simulation results are analyzed and discussed based on the internal flow behavior within the impeller and fluid domain. An experimental analysis is also carried out with both the pumps to get the performance parameters for the experimental operating range, i.e., the shut-off to maximum flow rate. The results are discussed below.

5.1. Results of numerical simulation

The numerical analysis is used to evaluate and compare the internal flow behavior of the optimized pump and the base pump. The characteristics of pump performance are measured with contour plots for $0.6 Q_d$, $0.8 Q_d$, $1 Q_d$, and $1.20 Q_d$ flow conditions. Fig. 4 depicts the static pressure distribution at the mid-span of impeller and volute for the base and optimized pump under the design and off-design conditions. The pressure progressively rises along with the impeller blade path and reaches a peak at TE. As in the passage of the impeller, the mechanical energy is converted into the hydraulic energy of the fluid. Uniform pressure distribution is shown in the impeller flow path for the design flow, and non-uniform pressure distribution is visualized for the off-design flow near the blade's LE and TE areas. The pressure is lowest towards the blade's LE areas in the base pump and optimized pump (P_1 , P_1' , Q_1 , Q_1' , R_1 , R_1' , S_1 , and S_1' in Figs. 4(a)-(h), respectively), where cavitation may arise [24].

The pressure is uniformly distributed in the volute flow path and reaches the peak in the volute diffuser outlet. The convergence of kinetic energy to pressure energy of the fluid takes place into volute flow passage. The non-uniform pressure cloud is observed at the impeller-volute interaction (mixing) zone in the base pump, while the uniform one is visualized in the optimized pump (P_2 , P_2' , Q_2 , Q_2' , R_2 , R_2' , S_2 , and S_2' in Figs. 4(a)-(h), respectively). Despite the high pressure in the base pump volute, the secondary flow losses and the non-uniformity of the flow at the impeller outlet increase and the energy stratification decreases [3]. The result shows higher energy loss in the base pump rather than the optimized pump.

In the case of the base configuration, one can observe the same high-pressure contours near the outlet periphery of impeller blade passage as well as the inlet of volute passage (P_3 , Q_3 , R_3 , and S_3 in Figs. 4(a)-(d), respectively). At the same time, the pressure distribution is more uniform at the rotor-stator interaction zone in the optimized pump (P_3' , Q_3' , R_3' , and S_3' in Figs. 4(e)-(h), respectively). The non-uniform pressure contours at the rotor-stator interaction zone lead to the extreme pressure

pulsation, unsteady forces, and shock losses with vibration in the impeller [25]. Overall, a more uniform flow is observed at the optimized pump’s design and off-design condition than the base pump. However, the pressure distribution is more consistent at both impellers’ design conditions than off-design conditions.

The effect of the blade number (Z), blade exit angle (β_2°), and width ratio (b_3/b_2) on the vortex formation and losses in the mixing zone by velocity contours in volute and vectors in the impeller are represented in Fig. 5. The base model results in the high fluid flow velocity and the increased blade friction losses, whereas the optimum model enables the energy stratification inside the flow path and vortex formation near the impeller exit [3]. The intensity of the vortex is higher at a lower flow rate, which disappears at the design and high flow rate conditions [26]. (It is seen from Figs. 5(a), (b), (e), and (f), respectively.) The vortex formation in the impeller passages influences the pump’s developed pressure head and efficiency [27]. The higher velocity gradient at volute zone in the base model (L_1, M_1, N_1 , and O_1 in Figs. 5(a)-(d), respectively) results in the hydraulic excitation forces and more mixing losses than the optimized case (L_1', M_1', N_1' , and O_1' in Figs. 5(e)-(h), respectively). The uniform accelerating vector pattern observed following the impeller throat passage in the optimized pump ($1.0 Q_d$ and $1.2 Q_d$) and base pump ($1.2 Q_d$) illustrates the absence of vortex, reduction in hydraulic flow losses, and increase in efficiency. In general, the non-uniformity in flow-velocity is higher at the off-design flow than the design flow, which results in the generation of the vortex (Figs. 5(a), (b), (c), (e), and (f), respectively).

Fig. 6 reveals a higher value of total pressure in the base pump compared to the optimized pump. However, one can also observe high variations of total pressure across the zone of impeller-volute interaction ($A_1, A_2, B_1, B_2, C_1, C_2, D_1$, and D_2 in Figs. 6(a)-(d), respectively). It indicates more hydraulic losses in the base pump, whereas the more uniform total pressure is observed at the impeller-volute interaction zone for the optimized case ($A_1', A_2', B_1', B_2', C_1', C_2', D_1'$, and D_2' in Figs. 6(e)-(h), respectively). The higher the total pressure variation, the more the hydraulic losses [3].

Results suggest that the rise in pressure head is with the increase in blade number, the width ratio influences the mixing losses, and the smaller blade exit angle gives better performance of the pump. The optimized pump shows lower losses and better efficiency compared to the base pump because of the balance between the selected parameters.

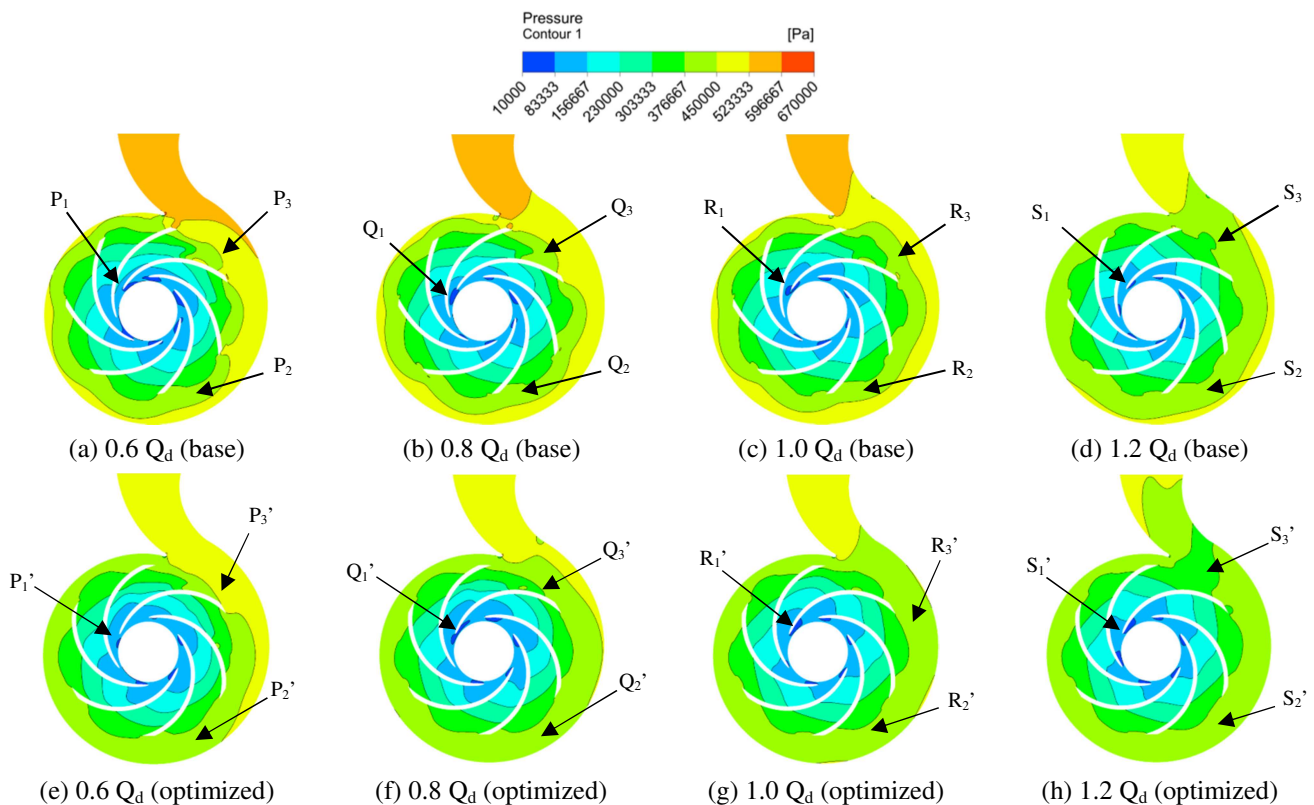


Fig. 4 Pressure distribution in the base and optimized pump impellers

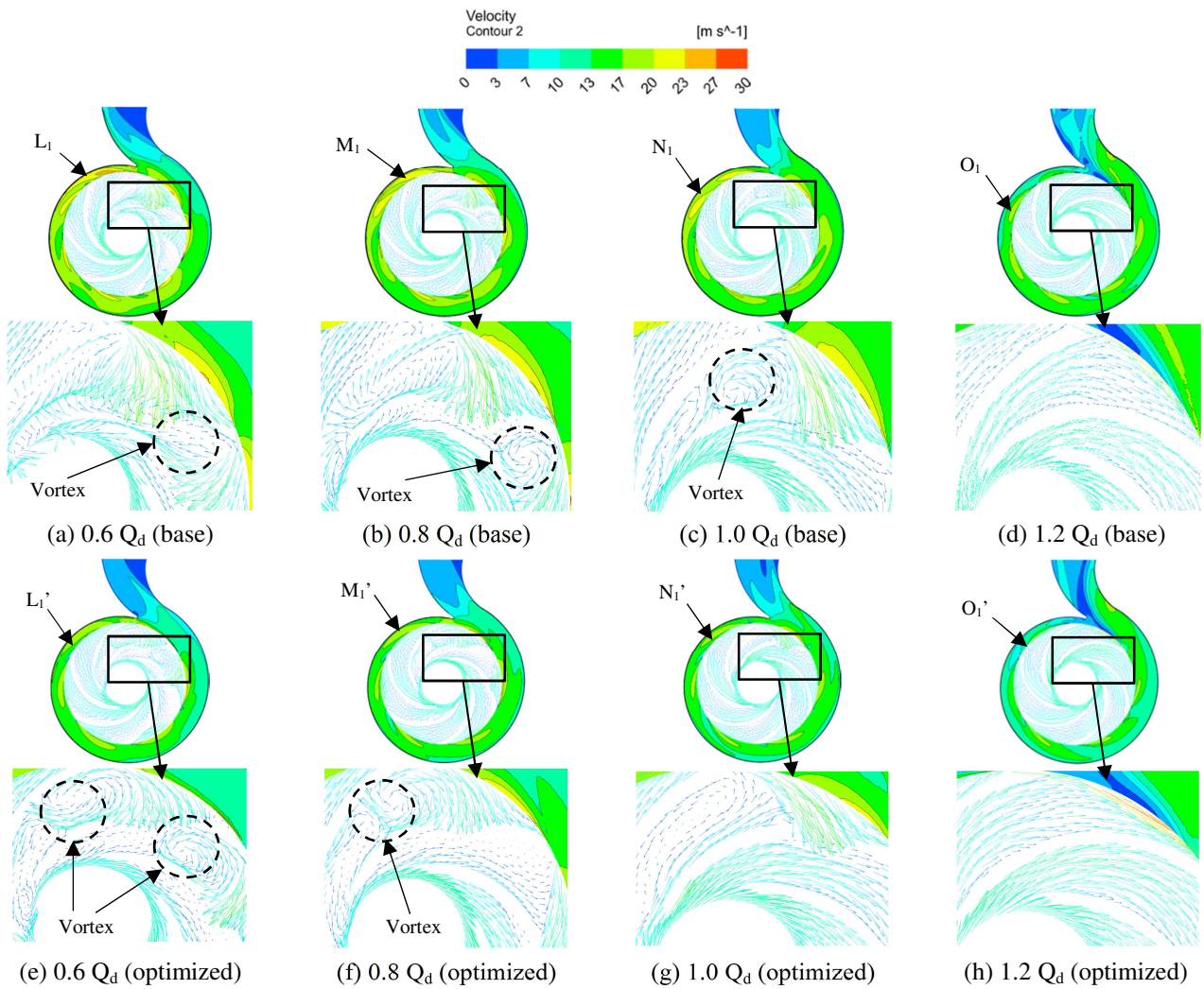


Fig. 5 Mid-span velocity distribution in the volute and vector distribution in the impeller of the base and optimized pumps

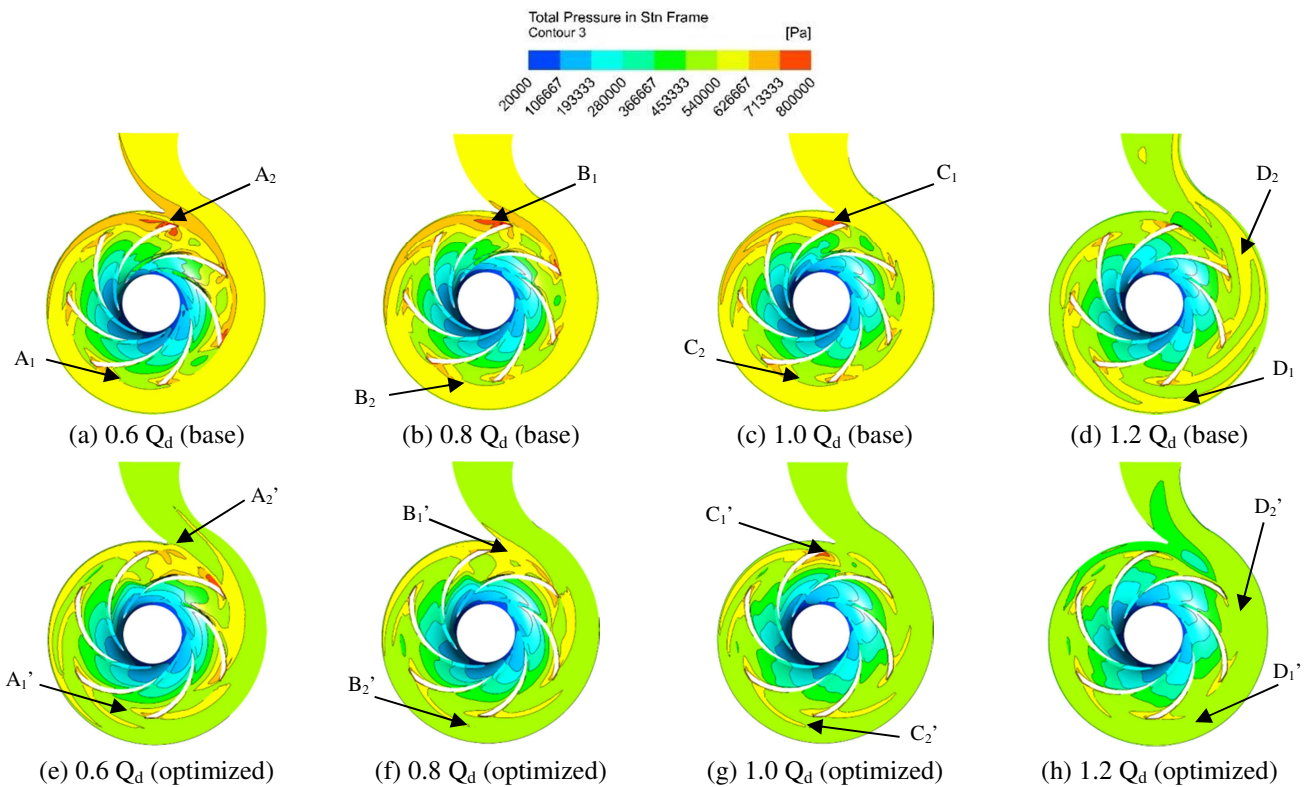


Fig. 6 Total pressure distribution in the volute and impeller mid-span of the base and optimized pump

5.2. Results of experimental analysis

The results of numerical analysis suggest better flow conditions in the optimized pump than the base pump. The experimental investigation is carried out to better understand the actual flow within the pump domain, and the results are plotted in a non-dimensional form. Tests are performed with the base and optimized centrifugal pump, as shown in Fig. 7. Both pumps have the same specific speed, and geometrical parameters except the parameters considered for optimization. Table 7 represents the variable geometric parameters details for the base and optimized centrifugal pump.

Experimental analysis is carried out in submerged conditions as per ISO 9906 for a complete operating range of centrifugal pumps, i.e., from shut-off to maximum flow conditions [16]. Fig. 8 represents the variation of the non-dimensional head for different non-dimensional mass flow rates throughout the operating range of the base and optimized pump. The figure reveals that the optimized pump covers a wider range of mass flow with a higher developed head than the base pump. At BEP, the optimized pump has the flow with $1.13 Q_d$ and head with $0.97 H_d$, which is higher about 10% and 5.4% of the base pump's flow and head, respectively.

The pump efficiency is calculated based on the ratio of pump output power to the pump input power [1]. The variation in efficiency at non-dimensional flow rates is shown in Fig. 9. One can observe a wider plateau of efficiency (η) curve in the case of the optimized pump. In the base one, the width of the plateau is reduced a lot. Better efficiency is observed in the case of the optimized pump compared to the base pump.

Fig. 9 reveals that the optimized pump efficiency (η) is 72% which is 12% higher than the base pump value, i.e., 60%, at BEP. The experimental readings show a high amount of power consumption by the base pump to achieve the desired output compared to the optimized pump. It leads to reducing the pump efficiency. The losses in the base pump indicate higher secondary flow losses at the impeller outlet to the volute inlet as justified in numerical results. The head and efficiency plots suggest better flow conditions and performance in the case of the optimized pump compared to the base one [16]. Therefore, one can summarize that an appropriate selection of optimization parameters helps enhance the pump's performance. Fig. 10 compares the numerical and experimental heads developed at four abreast flow rates. The figure suggests a minor deviation at a low flow rate, which increases at a higher flow rate. The maximum variation of 3.2% is observed for the flow rate $1.2 Q_d$.

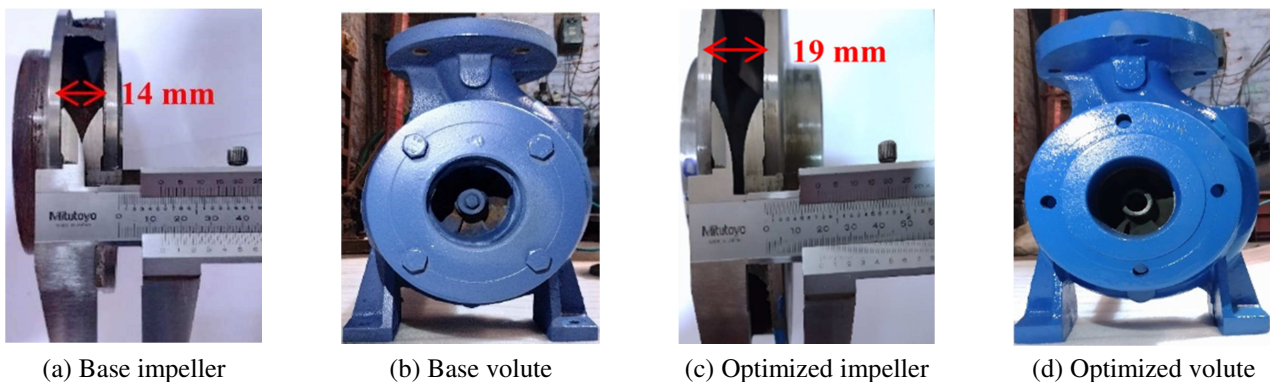


Fig. 7 The base and optimized centrifugal pump

Table 7 Details of variable geometrical parameters

Module	Parameters	Value	
		Base case	Optimized case
Impeller	b_2	14 mm	19 mm
	β_2	36°	19°
	Z	7 (nos.)	6 (nos.)
Volute	b_3	23 mm	38 mm
	b_3/b_2	1.64	2

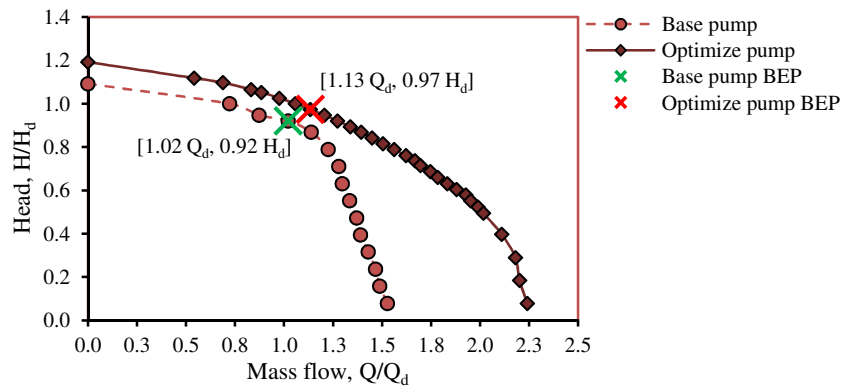


Fig. 8 Variation in non-dimensional mass flow v/s head

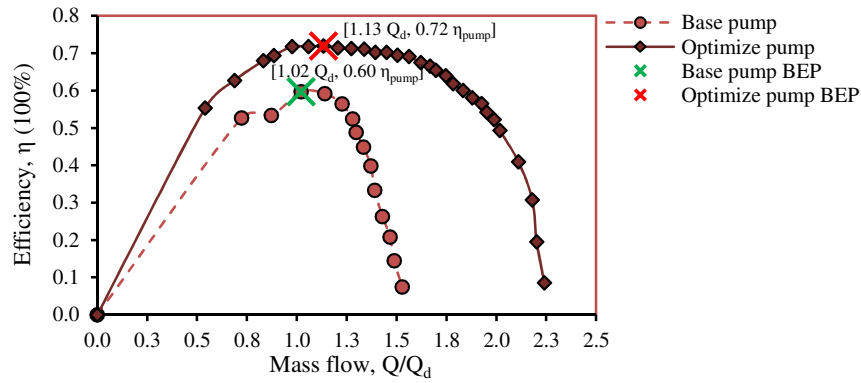


Fig. 9 Variation in non-dimensional mass flow v/s efficiency

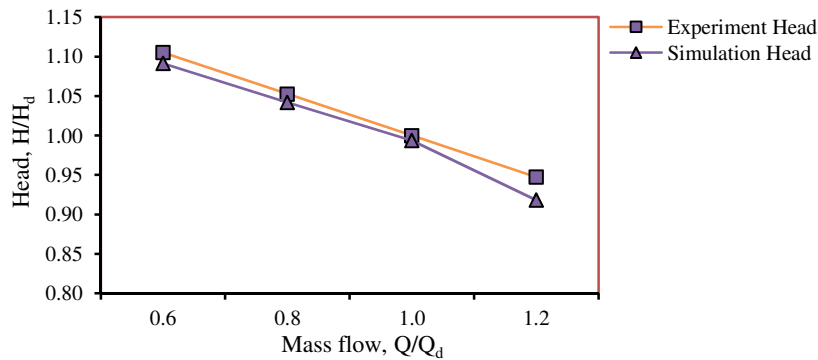


Fig. 10 Numerical and experimental head comparison of the optimized pump

6. Summary and Conclusions

In the present study, three design parameters are chosen for orthogonal design experiments, and the ideal combination of parameters is decided using numerical simulation data. The numerical results reveal that the pressure cloud generated between the rotor-stator interaction zone leads to the increased total pressure loss and high energy loss in the base pump. There is a significant impact of the vortex formation observed at low flow rates and diminished at high flow rates. The base and optimized pump's experimental performance are carried out to check the performance enhancement of the base pump by optimization. The finding of this study can be summarized as follows.

- (1) The width ratio b_3/b_2 has the most significant impact on the flow rate by minimizing the shock and secondary flow losses. Also, the number of blades Z strongly influences the head, and the blade outlet angle β_2 has a strong impact on the pump efficiency.
- (2) The optimized pump gives a wider range of operation with an increase of 10%, 5%, and 12% in flow rate, head, and efficiency, respectively, as compared to the base centrifugal pump.

Acknowledgments

The authors would like to thank Arvind Pumps Pvt. Ltd., Ahmedabad, India, for facilitating testing facilities.

Conflicts of Interest

The authors declare no conflict of interest.

References

- [1] G. Peng, S. Hong, H. Chang, Z. Zhang, and F. Fan, "Optimization Design of Multistage Pump Impeller Based on Response Surface Methodology," *Journal of Theoretical and Applied Mechanics*, vol. 59, no. 4, pp. 595-609, 2021.
- [2] S. H. Susilo and A. Setiawan, "Analysis of the Number and Angle of the Impeller Blade to the Performance of Centrifugal Pump," *EUREKA: Physics and Engineering*, vol. 2021, no. 5, pp. 62-68, September 2021.
- [3] G. R. A. Elyamin, M. A. Bassily, K. Y. Khalil, and M. S. Gomaa, "Effect of Impeller Blades Number on the Performance of a Centrifugal Pump," *Alexandria Engineering Journal*, vol. 58, no. 1, pp. 39-48, March 2019.
- [4] B. Shi, K. Zhou, J. Pan, X. Zhang, R. Ying, L. Wu, et al., "PIV Test of the Flow Field of a Centrifugal Pump with Four Types of Impeller Blades," *Journal of Mechanics*, vol. 37, pp. 192-204, 2021.
- [5] S. A. I. Bellary and A. Samad, "Improvement of Efficiency by Design Optimization of a Centrifugal Pump Impeller," *Proc. of ASME Turbo Expo: Turbine Technical Conference and Exposition*, pp. 1-11, June 2014.
- [6] D. Wu, P. Yan, X. Chen, P. Wu, and S. Yang, "Effect of Trailing-Edge Modification of a Mixed-Flow Pump," *Journal of Fluids Engineering*, vol. 137, no. 10, 101205, October 2015.
- [7] Y. Zhang, S. Hu, J. Wu, Y. Zhang, and L. Chen, "Multi-Objective Optimization of Double Suction Centrifugal Pump Using Kriging Metamodels," *Advance in Engineering Software*, vol. 74, pp. 16-26, August 2014.
- [8] S. Derakhshan and N. Kasaeian, "Optimization, Numerical, and Experimental Study of a Propeller Pump as Turbine," *Journal of Energy Resources Technology*, vol. 136, no. 1, 012005, March 2014.
- [9] Y. Xu, L. Tan, S. Cao, and W. Qu, "Multiparameter and Multiobjective Optimization Design of Centrifugal Pump Based on Orthogonal Method," *Proc. of the Institution of Mechanical Engineers, Part C: Journal of Mechanical Engineering Science*, vol. 231, no. 14, pp. 2569-2579, July 2017.
- [10] Z. Li, H. Ding, X. Shen, and Y. Jiang, "Performance Optimization of High Specific Speed Centrifugal Pump Based on Orthogonal Experiment Design Method," *Processes*, vol. 7, no. 10, 728, October 2019.
- [11] Y. Sekino and H. Watanabe, "Design Optimization of Double-Suction Volute Pumps," *World Pumps*, vol. 2016, no. 5, pp. 32-35, May 2016.
- [12] J. H. Kim, B. M. Cho, Y. S. Kim, Y. S. Choi, K. Y. Kim, J. H. Kim, et al., "Optimization of a Single-Channel Pump Impeller for Wastewater Treatment," *International Journal of Fluid Machinery and Systems*, vol. 9, no. 4, pp. 370-381, October-December 2016.
- [13] D. O. Baun and R. D. Flack, "Effects of Volute Design and Number of Impeller Blades on Lateral Impeller Forces and Hydraulic Performance," *International Journal of Rotating Machinery*, vol. 9, no. 2, pp. 145-152, 2003.
- [14] A. J. Stepanoff, *Centrifugal and Axial Flow Pumps: Theory, Design, and Application*, Florida: Krieger Publishing Company, 1993.
- [15] H. Alemi, S. A. Nourbakhsh, M. Raisee, and A. F. Najafi, "Effects of Volute Curvature on Performance of a Low Specific-Speed Centrifugal Pump at Design and Off-Design Conditions," *Journal of Turbomachinery*, vol. 137, no. 4, 041009, April 2015.
- [16] C. Wang, Y. Zhang, H. Hou, Z. Yuan, and M. Liu, "Optimization Design of an Ultra-Low Specific-Speed Centrifugal Pump Using Entropy Production Minimization and Taguchi Method," *International Journal of Fluid Machinery and Systems*, vol. 13, no. 1, pp. 55-67, January-March 2020.
- [17] *End-Suction Centrifugal Pumps (Rating 16 Bar)—Designation, Nominal Duty Point and Dimensions*, ISO 2858, 2017.
- [18] W. Wang, M. K. Osman, J. Pei, S. Yuan, J. Cao, and F. K. Osman, "Efficiency-House Optimization to Widen the Operation Range of the Double-Suction Centrifugal Pump," *Complexity*, vol. 2020, 9737049, 2020.
- [19] A. F. Ayad, H. M. Abdalla, and A. A. E. A. Aly, "Effect of Semi-Open Impeller Side Clearance on the Centrifugal Pump Performance Using CFD," *Aerospace Science and Technology*, vol. 47, pp. 247-255, December 2015.
- [20] M. Jeon, T. T. Nguyen, H. K. Yoon, and H. J. Cho, "A Study on Verification of the Dynamic Modeling for a Submerged Body Based on Numerical Simulation," *International Journal of Engineering and Technology Innovation*, vol. 10, no. 2, pp. 107-120, March 2020.

- [21] J. F. Gülich, *Centrifugal Pumps*, New York: Springer, 2008.
- [22] *Rotodynamic Pumps—Hydraulic Performance Acceptance Tests—Grades 1 and 2, ISO 9906*, 2012.
- [23] S. Kline and F. McClintock, “Describing Uncertainties in Single-Sample Experiments,” *Mechanical Engineering*, vol. 75, pp. 3-8, 1953.
- [24] W. Wang, Y. Li, M. K. Osman, S. Yuan, B. Zhang, and J. Liu, “Multi-Condition Optimization of Cavitation Performance on a Double-Suction Centrifugal Pump Based on ANN and NSGA-II,” *Processes*, vol. 8, no. 9, 1124, September 2020.
- [25] G. Hongyu, J. Wei, W. Yuchuan, T. Hui, L. Ting, and C. Diyi, “Numerical Simulation and Experimental Investigation on the Influence of the Clocking Effect on the Hydraulic Performance of the Centrifugal Pump as Turbine,” *Renewable Energy*, vol. 168, pp. 21-30, May 2021.
- [26] X. Li, B. Chen, X. Luo, and Z. Zhu, “Effects of Flow Pattern on Hydraulic Performance and Energy Conversion Characterisation in a Centrifugal Pump,” *Renewable Energy*, vol. 151, pp. 475-487, May 2020.
- [27] R. Tao, X. Zhao, and Z. Wang, “Evaluating the Transient Energy Dissipation in a Centrifugal Impeller under Rotor-Stator Interaction,” *Entropy*, vol. 21, no. 3, 271, March 2019.



Copyright© by the authors. Licensee TAETI, Taiwan. This article is an open access article distributed under the terms and conditions of the Creative Commons Attribution (CC BY-NC) license (<https://creativecommons.org/licenses/by-nc/4.0/>).